Pseudo-Lithium Vacancies in Hydrogen Rich Li_3OCl

Benjamin A. D. Williamson,[1,*] Kristoffer Eggestad,[1] and Sverre M. Selbach[1]

[1]Department of Materials Science and Engineering,
NTNU Norwegian University of Science and Technology, Trondheim, Norway

The antiperovskite Li_3OCl is a Li-ion solid electrolyte that has shown a wide variety of properties over a large range of temperatures. Previous reports align Li_3OCl as a superionic conductor, however reproducibility has been poor due to its hygroscopic nature suggesting that reports are in fact, $Li_{3-x}OH_xCl$. Most studies in the literature focus on pure Li_3OCl however, and do not take into account the role of hydrogen in the material. Here, we develop a full defect model of H-doped Li_3OCl, showing that the nominal Schottky disorder diminishes with hydrogen incorporation. Additionally, H helps to facilitate Li-ion mobility in Li_3OCl by firstly introducing rotatable OH species as well as forming H_{Li} which relaxes off site to form what we define as a "pseudo-V_{Li}" enhancing the ionic conductivity in line with experimentally observed values. Intentional hydrogen doping of hygroscopic materials constitute an underexplored strategy for enhancing ionic transport properties.

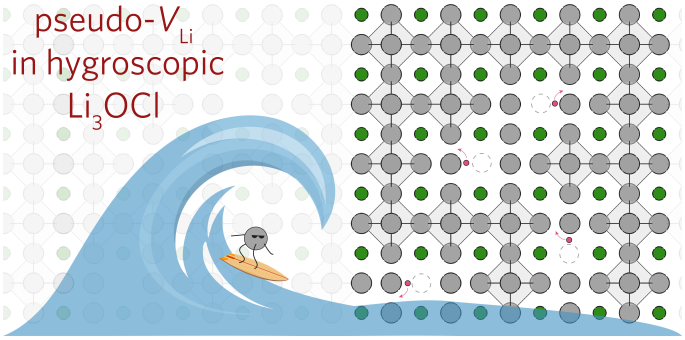

1. INTRODUCTION

Electrochemical energy storage has become an increasingly vital component of modern society ever present in both portable electronics and transportation, as well as becoming important in the realisation of a fully renewable energy grid. The dominating type ofrechargeable battery rely on Li-ions which intercalating into an anode upon charging, typically graphitic[1], migrate back to a cathode (for example: $LiCoO_2$[2], $LiFePO_4$[3,4] (LFP), or $LiNi_xMn_yCo_{1-x-y}O_2$ (NMC)[5]) upon discharging, and a liquid/polymer electrolyte such as LiTFSI.[6] These electrolytes typically possess desirable conductivities[7] of the order of $10^{-2}\,S\,cm^{-1}$. However, they present significant safety risks due to their flammable nature. Further disadvantages are formation of potentially rate limiting solid-electrolyte interphases, simultaneous anion diffusion[8], lower operating voltages[9], and dendrite formation causing incompatibility with Li-metal anodes with $\sim 10\times$ the capacity of current graphitic anodes[10]).[11] The use of a solid-state electrolyte (SSE) is therefore desirable as it fixes many of these problems simultaneously.

Current solid electrolyte materials include e.g. the Li-rich garnets such as $Li_7La_3Zr_2O_{12}$ (LLZO)[12–14], the Argyrodites Li_6MS_5X (M=S,Se,X=Cl,Br,I)[15–17], $Li_{10}GeP_2S_{12}$ (LGPS)[18–20], as well as $Li_xP_yO_zN$ (LiPON)[21,22]. Unfortunately, these materials possess a tradeoff between stability and conductivity. LiPON, for example, possesses excellent electrochemical stability and resistance towards dendrite formation[23], yet poor/mediocre conductivities of the order of $10^{-6}\,S\,cm^{-1}$ are typically observed[21]), making it suitable for small scale devices or as a protective layer in conventional lithium battery cells.[24] Whilst a lower conductivity would intuitively be expected in the solid state compared to the liquid state, competitively high conductivities ($>10^{-3}\,S\,cm^{-3}$) are observed for some solid state materials.[25] However, some expected issues do arise with respect to stability and synthesis of these materials.[8]

Within the past decade, Li-rich anti-perovskites, such as Li_3OCl have gained a lot of interest due to their initial high reported ionic conductivities at ambient conditions ($10^{-3}\,S\,cm^{-1}$) as reported by Zhao and Daemen[26]. Subsequent experimental and density functional theory (DFT) studies, however, have placed the conductivity to be much lower with a higher migration barrier($\sim 0.6\,eV$ and $10^{-6}\,S\,cm^{-1}$[27,28]). Both nominally Li_3OCl and Li_3OBr have been shown to possess wide electrochemical stability windows even if they are metastable and not in a global ground state. This has been attributed due to its lack of reducible cations to Li-metal, yet may form Li_2O and LiCl/Br at the anode.[29] Additional antiperovskite ionic conductor compositions have been reported including, Na_3OCl/Br[30,31], Na_3SI[32] and Na_3HS[33] to name a few.

* benjamin.williamson@ntnu.no

Despite promising electrochemical stability and sometimes promising ionic conductivities, Li_3OCl is a hygroscopic and air sensitive material.[28] This has raised numerous questions on the legitimacy of Li_3OCl as the true composition, with concensus trending towards the fact that Li_3OCl being a hydrated form ($Li_{3-x}OH_xCl$) or even Li_2OHCl.[28,34] In a critical review by Rettenwander and coworkers[34], they point out the fact that typical syntheses of Li_3OCl uses LiH, H_2O, or LiOH within the synthesis, thus it is inevitable that H/OH will be present in "Li_3OCl". All may not be lost, however, after several experimental and computational studies show that a hydrated composition may be to the advantage of the ionic conductivity, as rotatable OH units enhance the mobility of Li-species in the material.[35] Ultimately this may come at a cost, as the conductivity has been shown to be highly correlated with the proton and lithium vacancy concentration[36], and controlling the amount of hydrogen in a hygroscopic material is difficult at best.[34] Whilst computational studies exist on the intrinsic defects of Li_3OCl[29,32,37–40], including a full defect model by Squires et al.[41], hydrogen has not previously been fully included in the defect model. Squires et al. show that purely undoped Li_3OCl is an extended Schottky disordered material ($[V_{Li}+V_{Cl}+O_{Cl}]$), similar to what is seen in previously calculated models $[V_{Li}+V_{Cl}]$[41], which Mouta et al. showed to enhance the ionic conductivity of Li_3OCl.[40] Squires also showed that undoped Li_3OCl could expect equilibrium ionic conductivities of $\sim 10^{-10}\,S\,cm^{-1}$, significantly below experimental observations.[28]

Here, we present full intrinsic and extrinsic (H) defect models for metastable Li_3OCl, calculated with the hybrid functional HSE06. Using the quasiharmonic approximation, the chemical potential stability region of Li_3OCl is shown to exist from $\sim$ 750 K and shows that when undoped, Li_3OCl displays two types of Schottky disorder: full disorder under Li-rich conditions, and Li_2O disorder under Li-poor conditions. Hydrogen is shown to incorporate very easily, in line with the hygroscopic nature of Li_3OCl, and suppresses these Schottky defect clusters. Additionally, lithium substituted hydrogen is likely to relaxe offsite to form OH groups and induce a "pseudo-V_{Li}". Accounting for this defect in a conductivity model reproduces experimentally observed values.

2. COMPUTATIONAL METHODS

Ab-initio calculations were performed using density functional theory (DFT) implemented within the plane-wave periodic code, VASP.[42–45] The projector-augmented wave method (PAW)[46,47] was used to describe the interaction between the core electrons and the valence electrons. All electrons were treated explicitly for Li, while for O, Cl, Br and H the standard pseudopotentials supplied with VASP were used. The hybrid functional HSE06 (Heyd-Scuseria-Ernzerhof)[48] was used in order to address the self-interaction error thus allowing for an accurate description of the band gap and electronic properties of Li_3OCl.

Hybrid functionals have consistently displayed improved geometry and electronic properties of semiconductors.[13,49–51] The band gap calculated herein is $\sim$6.6 eV which aligns well with previous HSE06 studies ($\sim$6.4-6.6 eV)[41,51,52]. To date, however, there is no experimental band gap with which to compare.

Determination of the bulk electronic and structural properties were performed on the cubic form (5 atom primitive cell) of Li_3OCl and Li_3OBr (space group: $Pm\bar{3}m$). To this end, a full geometric relaxation using a Γ-centred k-point grid of $6 \times 6 \times 6$ and a plane wave energy cutoff of 500 eV was carried until the largest force on any atom was below the force criterion of 0.01 eV Å^{-1}. The intrinsic defects were simulated using a $3 \times 3 \times 3$ supercell expansion of the conventional cell containing 135 atoms. Spin-polarised geometry relaxations (to the same convergence criteria as the conventional cell) of each defect cell and its respective charge states were performed using a Γ-centred 2×2×2 k-point mesh and 500 eV plane wave energy cutoff. A Γ-centred k-point 2×2×2 mesh was chosen in order to capture the M-point in the 1^{st} Brillouin zone, which is the valence band maximum (VBM) and conduction band minimum (CBM) (SI Figure S1), which was not captured in a Monkhorst-Pack 2×2×2 grid. The bulk electronic and structural properties are given in the supporting information (Secions SI 2, and SI 1).

2.1. Defect Formalism

Equation 1 describes the enthalpy of formation of a defect in charge state q:

$$\begin{aligned}\Delta H_f(D,q) =&(E^{D,q} - E^H) + \sum_i n_i(E_i + \mu_i) + \\ & q(E_{\text{Fermi}} + \epsilon^H_{VBM} + \Delta\, E^{\text{pot}}) \\ & + q^2 E^{IC}_{\text{corr}} + E^{BF}_{\text{corr}}\end{aligned} \tag{1}$$

Where E^{H} is the total energy of the host supercell, $E^{D,q}$ is the total energy of the defective supercell in charge state q. E_i corresponds to an elemental reference energy ($Li_{(s)}$, $Cl_{(s)}$, $O_{2(g)}$ and $Br_{2(s)}$) and has an associated chemical potential denoted by μ_i. n refers to the number of element i added to or taken away from an external reservoir[53]. In this work, the Fermi level ranges from the valence band maximum (VBM) at 0 eV (where ϵ^H_{VBM} denotes the eigenvalue of the VBM in the host material) to the conduction band minimum (CBM) which occurs at 6.38 eV. The potential of the defect supercell bar the immediate vicinity of the defect is averaged and aligned to the host supercell and is described by $\Delta\, E^{\text{pot}}$.[54]

To account for the finite size effects of the defect supercells, two post-processing corrections are applied, E^{IC}_{corr} and E^{BF}_{corr}. The first correction term corresponds to the image-charge correction which minimises the long

ranged nature of the Coulomb interaction[55,56] of the charged defect and its periodic images. The implementation used herein uses a formalism based upon the Lany and Zunger correction[54] with a 'non-cubic' adaptation as implemented by Hine and Murphy.[56,57] Lastly a band-filling correction is applied to shallow and resonant defects to account for the high carrier concentrations present in supercell calculations so as to regain the 'dilute limit'.[54,58]

2.2. Equilibrium Concentrations

Equilibrium concentrations of defects in both Li_3OCl and Li_3OBr can be calculated self-consistently as implemented in the code `SC-FERMI`[59]. By determining the Fermi energy self-consistently the concentration of a defect D in charge state q can be evaluated through:

$$[D,q] = N_D g_{D,q} \exp(\frac{-\Delta H(D,q)}{kT}) \quad (2)$$

where N_D, $g_{D,q}$ and $\Delta H(D,q)$ are the number of sites on which the defect can form, the degeneracy of the defect state and the enthalpy of formation of the defect as calculated in equation 1 respectively. Given a constraint of overall charge neutrality, the electron and hole concentrations can be determined from equations 3 and 4:

$$n_0 = \int_{E_g}^{\infty} f_e(E)\rho(E)dE \quad (3)$$

$$p_0 = \int_{-\infty}^{0} f_h(E)\rho(E)dE \quad (4)$$

where $\rho(E)$ is the density of states (DOS), E_g is the band gap and f_e is the Fermi-Dirac distribution function given by $f_e = [\exp(\frac{(E_F-E)}{kT}) + 1]^{-1}$ and $f_h = 1 - f_e(E)$. This approach has successfully been applied to $Li_7La_3Zr_2O_{12}$[13] (LLZO) and elsewhere.[49,60]

3. RESULTS

3.1. Defining a Chemical Potential Stability Region for Metastable Li_3OCl

Determination of the formation energies of defects in materials requires knowledge of the individual elemental chemical potentials (equation 1) which are typically constrained by the thermodynamic stability of the host material relative to competing phases. As Li_3OCl is metastable and not globally stable, calculating the chemical potentials requires either prior experimental knowledge about phase stability[41], or calculation of host and competing phases at finite temperatures.[61] As the structure and composition of Li_3OCl is not widely acknowledged, the latter is chosen in this instance, however it is important to note that studies exist showing Li_3OCl to possess kinetic stabilty relative to LiCl and Li_2O[29,62], proposed to be due to the "sluggish" anion transport in Li_3OCl[63]. In this study, the chemical potential limits analysis program (CPLAP[64]) is combined with the quasi-harmonic approximation (QHA) to determine the temperature dependent stability region of Li_3OCl and thus unveil suitable chemical potentials without a-priori knowledge. This approach, whilst not widely used due to its increased computational expense, has shown recent success in determining the stability of $Na_2Ti_3O_7$.[61] From our results, Li_3OCl becomes the dominant phase at 750K/476.85°C (HSE06 functional), which agrees well with the expected experimental synthesis temperature from nominally non-hydrogen containing precursors, Li_2O and LiCl at (773K/500°C)[34]:

$$Li_2O + LiCl \xrightarrow{500\,^\circ C} Li_3OCl \quad (5)$$

Typically, however, Li_3OCl is often formed via a solid state synthesis from a combination of LiCl and LiOH at lower temperatures[26]:

$$LiCl + 2\,LiOH \xrightarrow[\text{high vacuum, several days}]{330\text{-}360\,^\circ C} Li_3OCl + H_2O \quad (6)$$

An overview of the common synthesis routes is given in SI Section 6 together with their calculated Gibbs free energy of reaction (ΔG_{reac}). Rettenwander and coworkers[34] showed that LiCl is still present after following the synthesis outlined in equation 6 suggesting that Li_3OCl is Cl-poor. This indicates that OH^- is likely present in the samples due to an excess of LiOH.[34]
Nevertheless, a calculated stability region can be formed and is given in Figure 1. What is seen is a very narrow region (straight line) between Li-rich/anion-poor ($\mu_{Li} = -2.17\,eV$, $\mu_O = 0\,eV$, $\mu_{Cl} = -2.97\,eV$) designated point A, and Li-poor/anion-rich (($\mu_{Li} = 0\,eV$, $\mu_O = -4.35\,eV$, $\mu_{Cl} = -5.14\,eV$)) designated point B. Whilst the results obtained from this method are somewhat strict, a larger region may be realised due to anion partial pressures. Anhydrous Li_3OCl can therefore be said to be stable over a more modest range of μ_{Li} than the larger μ_O and μ_{Cl}, anion deficiency or substitution in Li_3OCl is much more tolerated compared to Li deficiency, which could lead to thermodynamic instability towards other phases.
At point A, Li_3OCl is calculated to be in equilibrium with Li_2O, Li, and LiCl. At point B, Li_3OCl is in equilibrium with LiCl, Li_2O, and O_2.

3.2. Defect Thermodynamics

The thermodynamic transition levels as calculated with the HSE06 functional for Li_3OCl are plotted in Figure 2 showing both intrinsic (upper panels - (a) and (b)) and extrinsic hydrogen defects (lower panels (c) and (d)) at anion-poor/Li-rich conditions (point A, in Figure 1) and anion-rich/Li-poor conditions (point B in Figure 1) respectively. Additionally, the equilibrium concentrations

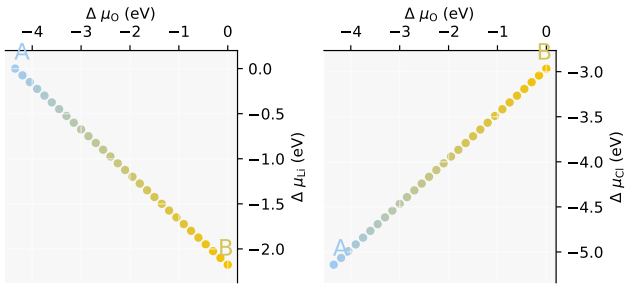

Figure 1: The chemical potential limits of Li and Cl as a function of O chemical potential as calculated using HSE06 within the QHA formalism at 750K. The chemical potential stability region is a thin area and is traversed by the coloured dots along μ_O from point A to point B.

of the dominant defects ($\geq 1 \times 10^8\,cm^{-3}$) are given in Figure 3 as a function of oxygen chemical potential (μ_O) as one travels from point A to point B. Even though hydrogen incorporation is typically unavoidable in Li_3OCl we will still refer to it as "doping" for the case of simplicity in this work.

Intrinsic Defects: The intrinsic defects of Li_3OCl are given in Figure 2(a) and (b) for Li-rich and Li-poor conditions respectively. Equilibrium concentrations when undoped and under H-doping are given in Figure 3(a) and (b) respectively. Under both regimes, lithium vacancies (V_{Li}) are the dominating defect possessing a formation energy of $\sim$ 1.02 eV at the Fermi level (E_F $\sim$3.71 eV and $\sim$1.37 eV for Li-rich and Li-poor conditions respectively when undoped). If we compare the Fermi level calculated at μ_O = -1.08 and -1.34 eV corresponding to the "experimentally accessible" oxygen chemical potentials of Li-rich and Li-poor conditions set out in the work by Squires et al.[41] we obtain formation energies of 2.05eV and 1.89 eV respectively in good agreement with their values of $\sim$2.20eV and $\sim$1.90eV. A thermodynamic determination of the "experimentally accessible" region of oxygen chemical potentials is given in SI Section 5. Upon H-doping, E_F increases in energy to $\sim$4.12 eV and $\sim$1.72 eV for Li-rich and Li-poor conditions respectively. Pushing E_F higher in energy, such as through doping[41] results in an ease in the formation of V_{Li}, increasing the concentration and therefore the ionic conductivity.

Under the most Li-rich/anion-poor conditions, point A, the dominant intrinsic defects are seen to be V_{Li}, V_{Cl}, and V_O, indicative of fully Schottky disorder. This is partially in agreement with previous literature findings[29,37,40,41] where three types of Schottky disorder are predicted, either "LiCl" partial Schottky: [V_{Li} + V_{Cl}], Li_2O partial Schottky: [$2V_{Li}$+V_O] or in the case of Squires et al.: [V_{Li}+V_{Cl}+O_{Cl}] (under Li-rich conditions).[37,40,41]. Contrary to Squires et al., however, in this work, both antisite defects, O_{Cl} and Cl_O, whilst forming in modest quantities, ($\sim 10^{12} - 10^{13}\,cm^{-3}$) are not expected to dominate the defect landscape of Li_3OCl. It is important to note that, O_{Cl} does increase to concentrations $\geq 10^{16}\,cm^{-3}$ upon H-doping, as seen in Figure 3 (c) simultaneously reducing [V_O], thus it could be said that the modified Schottky defect as calculated by Squires et al.[41] is somewhat valid. The fully Schottky defect calculated in this work is interesting in that V_{Cl} and V_O exist in the neutral (q=0) and partially ionised (q=1+) charge states respectively. Charge neutrality of the defect cluster is consequently caused by V_{Li} and V_O and can be defined in Kröger-Vink form as:

$$4Li_{Li}^{\times} + 4O_O^{\times} + 2Cl_{Cl}^{\times} \rightarrow 4V_{Li}' + 4V_O^{\bullet} + 2V_{Cl}^{\times} + 2Li_2O + O_2 + Cl_2 \quad (7)$$

As observed in the undoped concentrations in Figure 3 (a), [V_{Cl}] decreases rapidly between point A (anion poor) and point B (anion rich), and is not wholly influenced by H. This is in contrast to what is seen in Squires et al. where they show that the LiCl Schottky defect ([V_{Li}+V_{Cl}]) is predicted.

At the other extreme of the chemical potential stability region, under Li-poor conditions (point B), V_{Li} and V_O dominate. In the transition level diagram in Figure 2(b) it can be seen that V_O rises in energy such that it is in the 2+ charge state at E_F. The full Schottky defect in equation 7 at Li-rich conditions, thus becomes [$2V_{Li}$+ V_O]. In previous literature, this has been described as the Li_2O Schottky defect:[37,40]

$$2Li_{Li}^{\times} + O_O^{\times} \rightarrow 2V_{Li}' + V_O^{\bullet\bullet} + Li_2O \quad (8)$$

Counterintuitively, equilibrium [V_{Li}] under Li-rich conditions are higher than those under Li-poor conditions ($\sim 8 \times 10^{15}\,cm^{-3}$ vs $\sim 6 \times 10^{14}\,cm^{-3}$) despite the existence of neutral V_{Cl} under Li-rich conditions. Incidentally, interstitial Li (Li_i) will not be the dominant charge carrier over the entirety of the chemical potential range, which is echoed by previous literature[28], despite its lower migration barrier.[29] Despite this, it is expected that Li_i will be present, albeit in small quantities in undoped Li_3OCl ($\sim 7\times10^{13}\,cm^{-3}$) in a combined Schottky-Frenkel defect:

$$3Li_{Li}^{\times} + O_O^{\times} + V_i^{\times} \rightarrow 3V_{Li}' + V_O^{\bullet\bullet} + Li_i^{\bullet} + Li_2O \quad (9)$$

Upon H-doping, however, Li_i and V_O become suppressed as evident in Figure 3 (b) severely reducing both Li_2O

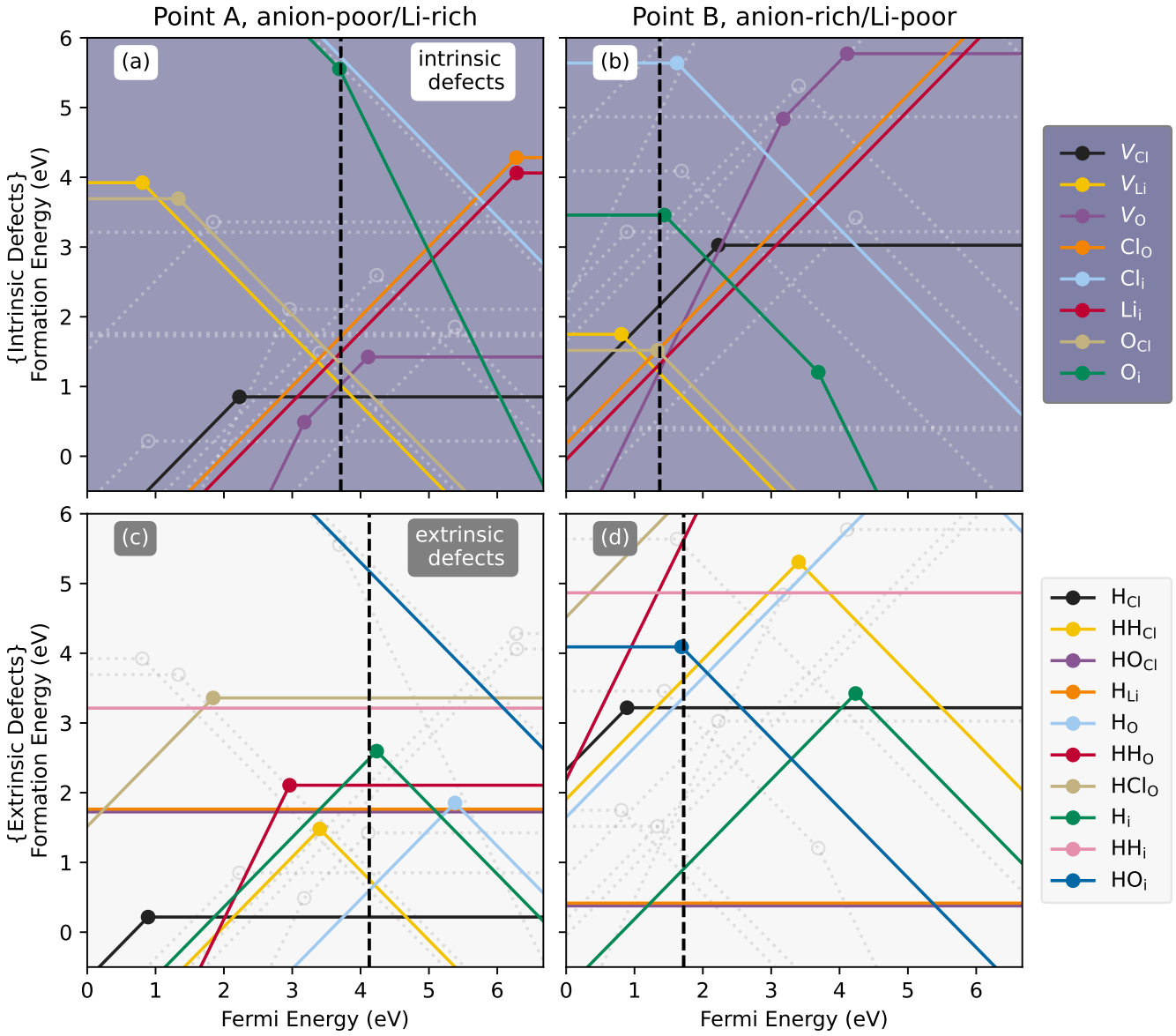

Figure 2: The thermodynamic transition levels for (a),(b) intrinsic defects and (c),(d) extrinsic H defects for the chemical potentials at points A (O-poor) and B (O-rich) respectively at 750 K, 1 atm. In each example the dashed vertical line represents the equilibrium Fermi level (E_F) and the corresponding extrinsic and intrinsic defects are shown by the faded dotted lines for reference.

Schottky and Schottky-Frenkel disorder under Li-poor conditions in Li_3OCl.

Extrinsic Hydrogen Defects: In this study, H-doping involving H, H_2, OH, and HCl defects are considered. The formation energies under Li-rich/anion-poor and Li-poor/anion-rich conditions are given in Figure 2 (c) and (d) respectively, and equilibrium defect concentrations in Figure 3 (c). In general, HCl and H_2 defects are high in energy and are not preferential to form, thus the thermodynamically favourable H-species are OH and singular H defects. This is in line with experimental suggestions that Li_3OCl is Cl-poor and OH rich.[34].

Under a Li-rich regime, the dominant H-defect is neutral H_{Cl} possessing a formation energy of $\sim$ 0.22 eV at E_F. This results in an equilibrium concentration of $\sim 2 \times 10^{21}\,cm^{-3}$. As previously stated, E_F is shifted further away from the VBM in the band gap from 3.71 eV to 4.13 eV upon H-incorporation. This has an additional role in lowering the cost of formation of V_{Li} from $\sim$ 1.02 eV to $\sim$ 0.60 eV thereby increasing its equilibrium concentration from $\sim 8 \times 10^{15}\,cm^{-3}$ to $\sim 5 \times 10^{18}\,cm^{-3}$. The next dominant hydrogen defect under Li-rich conditions is H_O. H_O forms at $\sim$ 0.60 eV at E_F, resulting in a concentration of $\sim 6 \times 10^{18}\,cm^{-3}$. Whilst H_{Cl} dominates

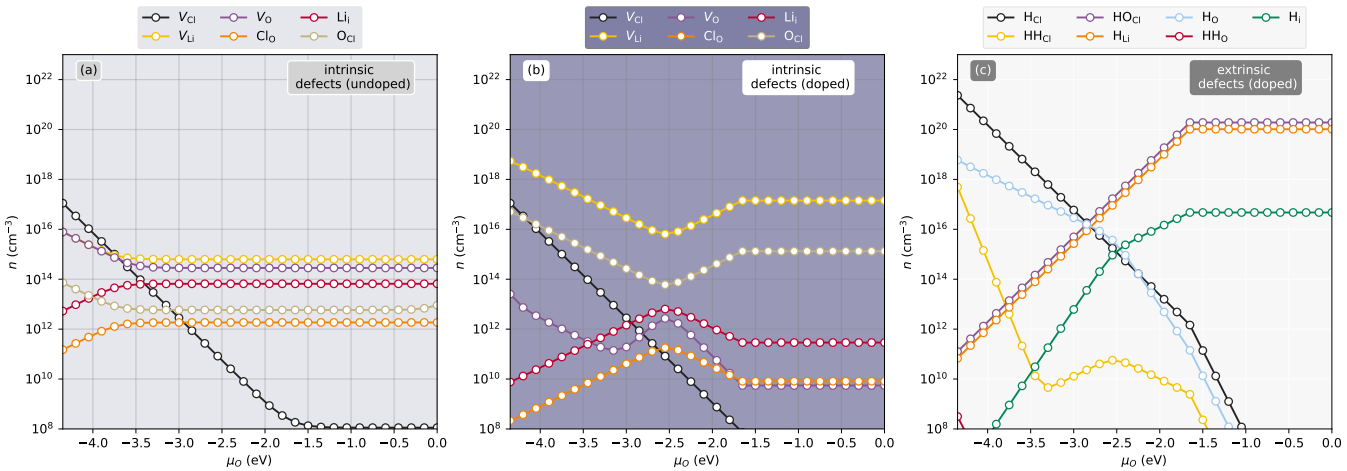

Figure 3: The equilibrium concentrations of all defects within Li_3OCl as a function of oxygen chemical potential (μ_O) with concentrations $> \times 10^5\,cm^{-3}$ as calculated at 750 K/1 atm. (a) shows the undoped intrinsic defect concentrations, whilst (b) and (c) show the intrinsic and extrinsic H-doped defect concentrations respectively.

at these conditions, it is H_O in the 1+ charge state that compensates V_{Li}. This results in a diminished $[V_O]$ compared to undoped Li_3OCl, and thus destruction of the full Schottky disorder as explained in equation 7. Towards Li-poor conditions both these defects tail off in favour of H_{Li} and OH_{Cl}, both neutral defects in themselves at $\mu_O = \sim -2.8\,eV$. It is expected, therefore that unintentional H-doping at these conditions results in an expected increase in mobile V_{Li} and thus ionic conductivity. $[Li_i]$ is reduced upon H-doping from $\sim 5 \times 10^{12}\,cm^{-3}$ to $\sim 8 \times 10^{9}\,cm^{-3}$. Under Li-rich conditions, the defect chemistry can be expressed as:

$$3H_2 + 4Li_{Li}^{\times} + 4O_O^{\times} + 2Cl_{Cl}^{\times} \rightarrow 4V_{Li}' + 4H_O^{\bullet} + 2H_{Cl}^{\times} + 2Li_2O + O_2 + Cl_2 \quad (10)$$

Towards Li-poor conditions (point B), H_{Li} and HO_{Cl} quickly become the dominant species with formation energies at E_F under point B of around 0.42 and 0.37eV respectively. As both defects are neutral (q=0), they aren't expected to be charge compensated by any intrinsic or otherwise H-related species. The equilibrium concentrations of $[H_{Li}]$ and $[HO_{Cl}]$ are fairly high $\sim 1 \times 10^{20}\,cm^{-3}$ and $\sim 2 \times 10^{20}\,cm^{-3}$ respectively. It is important to note, that whilst "equilibrium concentrations" are stated, we are constrained by the formation of Li_3OCl and it is highly likely that in reality excess H will make its way into the structure increasing H defect concentrations, or form additional $Li_{3-x}OH_xCl$ phases or Li_2OHCl. Upon H doping under Li-poor conditions, E_F again, shifts towards the conduction band minimum (CBM) from 1.37eV to 1.7eV resulting in a lower effective formation energy of V_{Li} from $\sim 1.18\,eV$ to $\sim 0.84\,eV$. As at point A, it is expected that $[V_{Li}]$ rises from $\sim 6 \times 10^{14}\,cm^{-3}$ when undoped to $\sim 1.4 \times 10^{17}\,cm^{-3}$.

Figure 4 (a) and (b) show the relaxed defect supercells of HO_{Cl} (at q=0), and H_{Li} (at q=0) respectively. HO_{Cl}, warps the structure shifting adjacent Li away from its preferred site (Wyckoff: 3c) towards the neutral cluster. As this defect is nominally neutral, the displacement arises due to the smaller OH^- radii (110pm) compared to Cl^- radii (181pm) and may aid in improving Li-ion transport by increasing "accessible space" and weakening the Li-O bonds. In H_{Li} (4 (b)), H shifts off its Li site (3c) towards an adjacent O forming a neutral OH. This defect can therefore be seen as a "pseudo-V_{Li}" or as suggested by Song et al.[65] a Frenkel-type defect as any moving Li into this space technically becomes an interstitial. Experimentally, Schwering et al.[66] suggested H_{Li} as the dominant defect, remarking also that H_{Li} provides rotatable OH that facilitates Li transport. Work carried out by Eilbracht et al.[67] using single crystal data on Li_2OHCl also suggest Li site occupation. Similar evaluations of the role of rotatable OH groups have been suggested in the literature.[36,65,68] Dawson et al.[36] using molecular dynamics simulations (MD) combined with ^2H NMR spectroscopy, observe that both highly rotatable OH groups exist alongside fixed OH groups. Further investigation shows that OH rotations are more free when O is coordinated to fewer lithiums.

4. DISCUSSION

In this study, we have performed hybrid functional charged defect calculations on H-doped Li_3OCl. This is in order to determine the influence of hydrogen on intrinsic defect chemistry of Li_3OCl and its influence on structure and ionic conductivity. In this model we have considered all vacancies, interstitials, antisites and varying H-related extrinsic species such as singular H, H_2, OH and HCl. A self-consistent model such as this is highly important for getting a holistic overview of the mechanisms for ionic conductivity as well unravelling the ther-

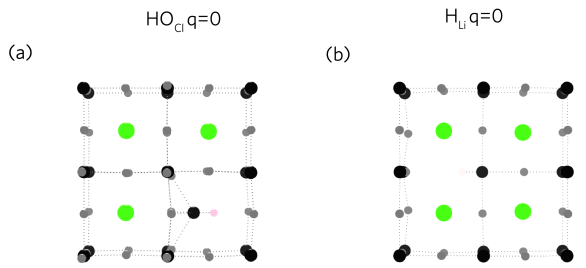

Figure 4: Relaxed defect structures of (a) HO_{Cl} (q=0), and (b) H_{Li} (q=0). In each example, lithium is coloured grey, chlorine is green, oxygen is black and hydrogen is pink. In (b), H_{Li} relaxes towards O forming a neutral OH species and forming a pseudo-V_{Li}.

modynamics of Li_3OCl as given in experimental and computational studies in previous literature.[29,32,36–40,65,68]

Taking a fully undoped Li_3OCl we find that across the range of synthesis conditions, (Li-poor to Li-rich), V_{Li} is the dominant charge carrying defect whilst Li_i exists in much lower concentrations, thus ruling out an interstitial or interstitialcy mechanism within Li_3OCl consistent with other reports[29,40,41,69], despite the lower migration energy barrier of 0.17eV (compared to 0.34eV for V_{Li}).[29] Under the most Li-rich/anion-poor conditions, the fully Schottky defect exists, [V_{Li}+V_O+V_{Cl}], however with V_{Cl} existing in the neutral charge state. This is somewhat contrary to previous reports of Li_3OCl being LiCl ([V_{Li}+V_{Cl}]) Schottky disordered.[29,38,41,70,71] It is important to note, however, that with the exception of the work in ref. [41], the other studies only consider neutral defects and assume full charge neutrality from V_{Li} and V_{Cl}, yet we find that the positive compensating defect for V_{Li} are oxygen vacancies (V_O). This changes to a Li_2O Schottky defect([V_{Li}+V_O]) under Li-poor conditions. Equally, whilst antisites are expected to form in small quantities ($\sim 10^{12} - 10^{13}\,cm^{-3}$) in a fully undoped Li_3OCl, our results do not point towards significant anion disorder.[18] Concensus in the literature is that anion disorder is beneficial to increasing the conductivity of Li-ion solid electrolytes. This is attributed to significant anion disorder opening up percolating three-dimensional pathways previously inaccessible to anion ordered systems.[15] In a paper by Li et al.[72] they stated that due to the size mismatch between O and Cl, anion antisite defects would cause a strong structural distortion and an electrostatic penalty for mobile lithium defects thus reducing the conductivity.

The inconsistency between this work and previous calculations is likely down to both the choice of functional, as well as from the calculation of the chemical potential stability region for Li_3OCl of which the defect formation energies are highly sensitive to. Hybrid functionals typically give a much better description of electron localisation for defects, as well as favourable description of the band gap of a material relative to experiment.[12,50,73,74] Both of these are crucial when determining charged defect calculations in order to correctly describe the thermodynamic defect quantities of solid electrolytes.[12,13,18,41] In this work, the chemical potential region was determined "temperature-dependently" through calculating the free energies of competing phases using QHA (Section 3 3.1), which has shown success previously in $Na_2Ti_3O_7$.[61] Confidence in this result arises from the fact that Li_3OCl becomes "stable" around $\sim$ 750K, in excellent agreement with the experimental synthesis temperature (without H) of $\sim$773K.[34]

The unfortunate reality of Li_3OCl is that it is highly unlikely to be purely Li_3OCl, but a hydrated form $Li_{3-x}OH_xCl$.[34,36] Even when attempting to create dehydrated forms of Li_3OCl, Li et al.[75] acknowledged that some form of OH is observable from FTIR. This work shows that hydrogen defects are omnipresent in the structure of Li_3OCl and high defect concentrations of at least $\geq 10^{20}\,cm^{-3}$ are to be expected. Our results indicate a baseline equilibrium which is likely to be higher based on both synthesis conditions and local atmosphere indeed forming Li_2OHCl. Nevertheless, our results do not rule out the formation of cubic anti-perovskite Li_3OCl without forming full Li_2OHCl compositions. Dawson et al. showed that hydrogen does not diffuse in Li_3OCl due to the large jump distances of 3.91Å.[36]

Under Li-rich conditions, it is expected that neutral H_{Cl} forms as the dominant defect which pushes E_F higher in energy towards the CBM thereby reducing the formation energy of V_{Li} within the crystal structure. At the same time, H-incorporation suppresses the Schottky disorder as seen in purely undoped Li_3OCl. This is also the case under Li-poor conditions, whereby the Li_2O Schottky disorder is cancelled by the neutral hydrogen defects: H_{Li} and OH_{Cl}. H_{Li} is seen to relax off its nominal Li site towards an adjacent oxygen forming an "OH_O" which can also be seen as a "pseudo-V_{Li}". Work by Schwering et al.[66] on Li_3OCl and Eilbracht et al.[67] on Li_2OHCl agree with this conclusion. This "pseudo-V_{Li}" can also be seen as a Frenkel defect, where the mobile Li becomes effectively an interstitial upon rotation of the OH species.[65] Additionally, OH_{Cl}, whilst neutral, acts to distort the structure slightly due to its smaller radii compared to Cl which may also aid Li mobility.

Squires et al.[41] calculated the conductivity of Li_3OCl within their full defect model through:

$$\sigma = \frac{Cq^2}{kT} D^* \tag{11}$$

Where C is the concentration of mobile ions, q is the charge of those ions, k the Boltzmann constant, T the temperature and the self-diffusion coefficient is given by D^* and takes into account the attempt frequency (1×10^{13} Hz), the hop distance (2.67Å[41]) and the migration barrier, E_m (0.34eV[29]).[41] In their work they showed that undoped Li_3OCl expects values of $\sim 10^{-10}\,S\,cm^{-1}$

far off the values present in experiment ($\sim 10^{-6} - 10^{-2}\,\mathrm{S\,cm^{-1}}$).[28]

Figure 5 displays the ionic conductivity as a function of μ_O calculated with the same strategy using our defect model for undoped and H-doped Li_3OCl. Our results align well with Squires et al. where low conductivities of $\sim 10^{-10}\,\mathrm{S\,cm^{-1}}$ are observed. Upon incorporation of hydrogen, the V_{Li} conductivity increases from $\sim 3.75 \times 10^{-11}\,\mathrm{S\,cm^{-1}}$ under Li-poor conditions to $\sim 3.35 \times 10^{-10}\,\mathrm{S\,cm^{-1}}$ under Li-rich conditions. By including the "pseudo-V_{Li}" into our model, before considering potential enhancements to the mobility due to OH rotations the ionic conductivity of H-doped Li_3OCl lie in the region of $\sim 10^{-6}\,\mathrm{S\,cm^{-1}}$ in better agreement with experiment. Work by Dawson et al. showed that lower concentrations of H within Li_3OCl resulted in lower migration energy barriers $\sim 0.30\,\mathrm{eV}$ whilst Song et al.[65] predicted values of $\sim 0.24/0.26\,\mathrm{eV}$. Whilst OH_{Cl} has an increased Li-coordination to H_{Li}, it is likely that OH_{Cl} may lower the barrier for migration in a similar way that Br does in $Li_3OCl_{1-n}Br_n$.[76]

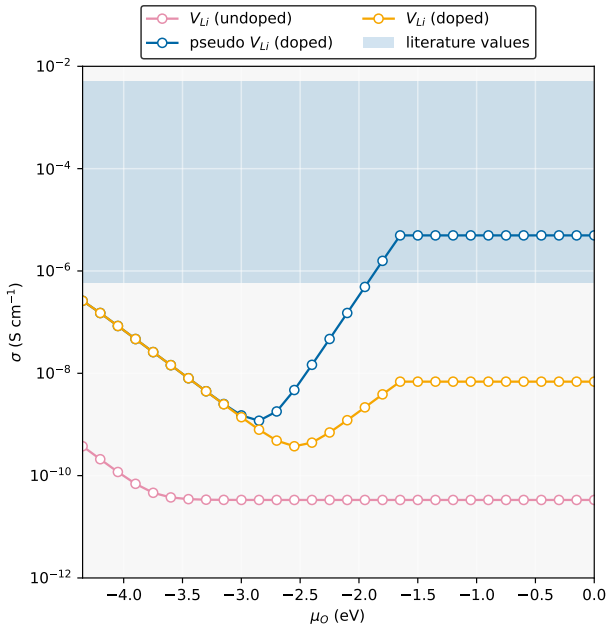

Figure 5: Room temperature ionic conductivity as a function of oxygen chemical potential taking into account the sum of v_{Li} and Li_i. Included is also the "pseudo" v_{Li} whereby H_{Li} is treated as a v_{Li} using the same migration barrier. A range of literature values is given, taken from reference [28].

5. CONCLUSIONS

In this work we illustrate the need for consideration of hydrogen as both a compositional changing opportunistic dopant, as well as a strategy for enhancing the ionic conductivity, not only in Li_3OCl but other hygroscopic solid electrolytes as well. A full defect model combined with a temperature dependent defined chemical potential stability region is necessary in order to outline doping strategies, killer defects, as well as structural changes in a given material. Our results highlight that, when undoped, Li_3OCl can expect a degree of Schottky disorder, both full and Li_2O-Schottky, in line with other computational predictions. Such a disorder, particularly anion disorder, can give rise to favourable ionic mobility of Li-species within the structure, similar to that in other solid electrolytes. Upon inevitable hydrogen incorporation, the Schottky disorder disappears, instead favouring the formation of neutral H species such as OH_{Cl} and H_{Li}. H_{Li} is shown to relax off site towards an adjacent oxygen forming an effective $[OH_O{+}V_{Li}]$ defect pair, or a "pseudo-V_{Li}". Considering only purely V_{Li} results in low ionic conductivities, however, upon consideration of a "pseudo-V_{Li}", our calculated ionic conductivities are more in line with experimentally observed values. Whilst Li_3OCl remains a controversial and challenging material, our results show that H may be a source of enhancement in Li_3OCl, increasing both the ionic mobility due to OH rotations, as well as increasing the effective carrier concentration.

6. ACKNOWLEDGEMENTS

This work was supported by the Research Council of Norway through Projects no. 275810 and 302506. Computational resources were provided by UNINETT Sigma2 through Projects NN9264K and ntnu243. B.A.D.W would like to acknowledge Nora S. Løndal and Caren R. Zeiger for useful discussions.

[1] T. Kim, W. Song, D.-Y. Son, L. K. Ono, and Y. Qi, J. Mater. Chem. A 7, 2942 (2019).
[2] K. Mizushima, P. C. Jones, P. J. Wiseman, and J. B. Goodenough, Materials Research Bulletin 15, 783 (1980).
[3] S. Geller and J. L. Durand, Acta Cryst 13, 325 (1960).
[4] J. Li and Z.-F. Ma, Chem 5, 3 (2019).
[5] H.-J. Noh, S. Youn, C. S. Yoon, and Y.-K. Sun, Journal of Power Sources 233, 121 (2013).

[6] Z. Huang, Z. Xiao, R. Jin, Z. Li, C. Shu, R. Shi, X. Wang, Z. Tang, W. Tang, and Y. Wu, Energy Environ. Sci. 17, 5365 (2024).
[7] D. Lu, Y. Shao, T. Lozano, W. D. Bennett, G. L. Graff, B. Polzin, J. Zhang, M. H. Engelhard, N. T. Saenz, W. A. Henderson, P. Bhattacharya, J. Liu, and J. Xiao, Advanced Energy Materials 5, 1400993 (2015).
[8] J. Janek and W. G. Zeier, Nat Energy 1, 1 (2016).
[9] X. Fan and C. Wang, Chemical Society Reviews 50, 10486 (2021).
[10] S. S. Park, S. A. Han, R. Chaudhary, J. H. Suh, J. Moon, M.-S. Park, and J. H. Kim, Advanced Energy and Sustainability Research 4, 2300074 (2023).
[11] I. T. Røe, S. M. Selbach, and S. K. Schnell, J. Phys. Chem. Lett. 11, 2891 (2020).
[12] K. Eggestad, S. M. Selbach, and B. A. D. Williamson, J. Mater. Chem. A (2024), 10.1039/D4TA01487A.
[13] A. G. Squires, D. O. Scanlon, and B. J. Morgan, Chem. Mater. 32, 1876 (2020).
[14] A. G. Squires, D. W. Davies, S. Kim, D. O. Scanlon, A. Walsh, and B. J. Morgan, Phys. Rev. Mater. 6, 085401 (2022).
[15] B. J. Morgan, Chem. Mater. 33, 2004 (2021).
[16] M. A. Kraft, S. P. Culver, M. Calderon, F. Böcher, T. Krauskopf, A. Senyshyn, C. Dietrich, A. Zevalkink, J. Janek, and W. G. Zeier, J. Am. Chem. Soc. 139, 10909 (2017).
[17] C. Yu, F. Zhao, J. Luo, L. Zhang, and X. Sun, Nano Energy 83, 105858 (2021).
[18] P. Gorai, H. Long, E. Jones, S. Santhanagopalan, and V. Stevanović, J. Mater. Chem. A 8, 3851 (2020).
[19] S. P. Ong, Y. Mo, W. D. Richards, L. Miara, H. S. Lee, and G. Ceder, Energy Environ. Sci. 6, 148 (2012).
[20] N. Kamaya, K. Homma, Y. Yamakawa, M. Hirayama, R. Kanno, M. Yonemura, T. Kamiyama, Y. Kato, S. Hama, K. Kawamoto, and A. Mitsui, Nature Mater 10, 682 (2011).
[21] V. Lacivita, A. S. Westover, A. Kercher, N. D. Phillip, G. Yang, G. Veith, G. Ceder, and N. J. Dudney, J. Am. Chem. Soc. 140, 11029 (2018).
[22] P. López-Aranguren, M. Reynaud, P. Głuchowski, A. Bustinza, M. Galceran, J. M. López del Amo, M. Armand, and M. Casas-Cabanas, ACS Energy Lett. 6, 445 (2021).
[23] F. Han, A. S. Westover, J. Yue, X. Fan, F. Wang, M. Chi, D. N. Leonard, N. J. Dudney, H. Wang, and C. Wang, Nat Energy 4, 187 (2019).
[24] S. Nowak, F. Berkemeier, and G. Schmitz, Journal of Power Sources 275, 144 (2015).
[25] Z. Zhang, Y. Shao, B. Lotsch, Y.-S. Hu, H. Li, J. Janek, L. F. Nazar, C.-W. Nan, J. Maier, M. Armand, and L. Chen, Energy & Environmental Science 11, 1945 (2018).
[26] Y. Zhao and L. L. Daemen, J. Am. Chem. Soc. 134, 15042 (2012).
[27] X. Lü, J. W. Howard, A. Chen, J. Zhu, S. Li, G. Wu, P. Dowden, H. Xu, Y. Zhao, and Q. Jia, Advanced Science 3, 1500359 (2016).
[28] J. A. Dawson, T. Famprikis, and K. E. Johnston, J. Mater. Chem. A 9, 18746 (2021).
[29] A. Emly, E. Kioupakis, and A. Van der Ven, Chemistry of Materials 25, 4663 (2013).
[30] T. H. Wan, Z. Lu, and F. Ciucci, Journal of Power Sources 390, 61 (2018).
[31] K. Hippler, S. Sitta, P. Vogt, and H. Sabrowsky, Acta Cryst C 46, 736 (1990).
[32] Z. Wang and G. Shao, Journal of Materials Chemistry A 5, 21846 (2017).
[33] S. Gao, T. Broux, S. Fujii, C. Tassel, K. Yamamoto, Y. Xiao, I. Oikawa, H. Takamura, H. Ubukata, Y. Watanabe, K. Fujii, M. Yashima, A. Kuwabara, Y. Uchimoto, and H. Kageyama, Nat Commun 12, 201 (2021).
[34] I. Hanghofer, G. J. Redhammer, S. Rohde, I. Hanzu, A. Senyshyn, H. M. R. Wilkening, and D. Rettenwander, Chem. Mater. 30, 8134 (2018).
[35] J. A. Dawson, T. S. Attari, H. Chen, S. P. Emge, K. E. Johnston, and M. Saiful Islam, Energy & Environmental Science 11, 2993 (2018).
[36] J. A. Dawson, T. S. Attari, H. Chen, S. P. Emge, K. E. Johnston, and M. S. Islam, Energy Environ. Sci. 11, 2993 (2018).
[37] Z. Lu, C. Chen, Z. M. Baiyee, X. Chen, C. Niu, and F. Ciucci, Physical Chemistry Chemical Physics 17, 32547 (2015).
[38] A. Baktash, B. Demir, Q. Yuan, and D. J. Searles, Energy Storage Materials 41, 614 (2021).
[39] Z. Zhang, Z. Ma, and Y. Pei, Phys. Chem. Chem. Phys. 25, 13297 (2023).
[40] R. Mouta, M. A. B. Melo, E. M. Diniz, and C. W. A. Paschoal, Chemistry of Materials 26, 7137 (2014).
[41] A. G. Squires, J. M. Dean, and B. J. Morgan, ChemRxiv (2021).
[42] G. Kresse and J. Hafner, Phys. Rev. B 49, 14251 (1994).
[43] G. Kresse and J. Hafner, Phys. Rev. B 47, 558 (1993).
[44] G. Kresse and J. Furthmüller, Computational Materials Science 6, 15 (1996).
[45] G. Kresse and J. Furthmüller, Phys. Rev. B 54, 11169 (1996).
[46] P. E. Blöchl, Phys. Rev. B 50, 17953 (1994).
[47] G. Kresse and D. Joubert, Phys. Rev. B 59, 1758 (1999).
[48] A. V. Krukau, O. A. Vydrov, A. F. Izmaylov, and G. E. Scuseria, J. Chem. Phys. 125, 224106 (2006).
[49] B. A. D. Williamson, J. Buckeridge, N. P. Chadwick, S. Sathasivam, C. J. Carmalt, I. P. Parkin, and D. O. Scanlon, Chem. Mater. 31, 2577 (2019).
[50] B. A. D. Williamson, T. J. Featherstone, S. S. Sathasivam, J. E. N. Swallow, H. Shiel, L. A. H. Jones, M. J. Smiles, A. Regoutz, T.-L. Lee, X. Xia, C. Blackman, P. K. Thakur, C. J. Carmalt, I. P. Parkin, T. D. Veal, and D. O. Scanlon, Chem. Mater. 32, 1964 (2020).
[51] M. Wu, B. Xu, X. Lei, K. Huang, and C. Ouyang, Journal of Materials Chemistry A 6, 1150 (2018).
[52] Y. Zhang, Y. Zhao, and C. Chen, Physical Review B 87, 134303 (2013).
[53] C. G. Van de Walle and J. Neugebauer, Journal of Applied Physics 95, 3851 (2004).
[54] S. Lany and A. Zunger, Phys. Rev. B 78, 235104 (2008).
[55] R. M. Nieminen, Modelling Simul. Mater. Sci. Eng. 17, 084001 (2009).
[56] N. D. M. Hine, K. Frensch, W. M. C. Foulkes, and M. W. Finnis, Phys. Rev. B 79, 024112 (2009).
[57] S. T. Murphy and N. D. M. Hine, Phys. Rev. B 87, 094111 (2013).
[58] C. Persson, Y.-J. Zhao, S. Lany, and A. Zunger, Phys. Rev. B 72, 035211 (2005).
[59] J. Buckeridge, Computer Physics Communications 244, 329 (2019).

[60] F. H. Taylor, J. Buckeridge, and C. R. A. Catlow, Chem. Mater. 28, 8210 (2016).
[61] Y.-S. Choi, S. I. R. Costa, N. Tapia-Ruiz, and D. O. Scanlon, ACS Appl. Energy Mater. 6, 484 (2023).
[62] M.-H. Chen, A. Emly, and A. Van der Ven, Physical Review B 91, 214306 (2015).
[63] J. a. S. Serejo, J. S. Pereira, R. Mouta, and L. G. C. Rego, Phys. Chem. Chem. Phys. 23, 6964 (2021).
[64] J. Buckeridge, D. O. Scanlon, A. Walsh, and C. R. A. Catlow, Computer Physics Communications 185, 330 (2014).
[65] A.-Y. Song, Y. Xiao, K. Turcheniuk, P. Upadhya, A. Ramanujapuram, J. Benson, A. Magasinski, M. Olguin, L. Meda, O. Borodin, and G. Yushin, Advanced Energy Materials 8, 1700971 (2018).
[66] G. Schwering, A. Hönnerscheid, L. van Wüllen, and M. Jansen, ChemPhysChem 4, 343 (2003).
[67] C. Eilbracht, W. Kockelmann, D. Hohlwein, and H. Jacobs, Physica B 234, 48 (1997).
[68] F. Wang, H. A. Evans, K. Kim, L. Yin, Y. Li, P.-C. Tsai, J. Liu, S. H. Lapidus, C. M. Brown, D. J. Siegel, and Y.-M. Chiang, Chem. Mater. 32, 8481 (2020).
[69] X. Lu, Y. Zhao, H. Xu, and Q. Jia, Abstracts of Papers of the American Chemical Society 250 (2015).
[70] Y. Zhang, X. He, Z. Chen, Q. Bai, A. M. Nolan, C. A. Roberts, D. Banerjee, T. Matsunaga, Y. Mo, and C. Ling, Nat Commun 10, 5260 (2019).
[71] J. A. Dawson, H. Chen, and M. S. Islam, J. Phys. Chem. C 122, 23978 (2018).
[72] P. Li, F. Hussain, P. Cui, Z. Li, and J. Yang, Phys. Rev. Materials 3, 115402 (2019).
[73] D. Broberg, K. Bystrom, S. Srivastava, D. Dahliah, B. A. D. Williamson, L. Weston, D. O. Scanlon, G.-M. Rignanese, S. Dwaraknath, J. Varley, K. A. Persson, M. Asta, and G. Hautier, npj Comput Mater 9, 1 (2023).
[74] M. Quesada-Gonzalez, B. A. D. Williamson, C. Sotelo-Vazquez, A. Kafizas, N. D. Boscher, R. Quesada-Cabrera, D. O. Scanlon, C. J. Carmalt, and I. P. Parkin, J. Phys. Chem. C 122, 714 (2018).
[75] Y. Li, W. Zhou, S. Xin, S. Li, J. Zhu, X. Lü, Z. Cui, Q. Jia, J. Zhou, Y. Zhao, and J. B. Goodenough, Angewandte Chemie International Edition 55, 9965 (2016).
[76] Z. Deng, B. Radhakrishnan, and S. P. Ong, Chemistry of Materials 27, 3749 (2015).